

Retrieving Jones matrix from an imperfect metasurface polarizer

Guanqing Zhang,^a Zixian Hu,^a Qichang Ma,^a Jiaming Huang,^a Junhong Deng,^b and Guixin Li^{a,c,d,*}

^aSouthern University of Science and Technology, Department of Materials Science and Engineering, Shenzhen, China

^bSouthern University of Science and Technology, Shenzhen Institute for Quantum Science and Engineering, Shenzhen, China

^cSouthern University of Science and Technology, Institute for Applied Optics and Precision Engineering, Shenzhen, China

^dSouthern University of Science and Technology, Guangdong Provincial Key Laboratory of Functional Oxide Materials and Devices, Shenzhen, China

Abstract. Optical metasurfaces, which consist of subwavelength scale meta-atoms, represent a novel platform to manipulate the polarization and phase of light. The optical performance of metasurfaces heavily relies on the quality of nanofabrication. Retrieving the Jones matrix of an imperfect metasurface optical element is highly desirable. We show that this can be realized by decomposing the generalized Jones matrix of a meta-atom into two parallel ones, which correspond to the ideal matrix and a phase retardation. To experimentally verify this concept, we designed and fabricated metasurface polarizers, which consist of geometric phase-controlled dielectric meta-atoms. By scanning the polarization states of the incident and transmitted light, we are able to extract the coefficients of the two parallel matrices of a metasurface polarizer. Based on the results of the Jones matrix decomposition, we also demonstrated polarization image encryption and spin-selective optical holography. The proposed Jones matrix retrieval protocol may have important applications in computational imaging, optical computing, optical communications, and so on.

Keywords: metasurface polarizer; Jones matrix; optical holography.

Received Sep. 6, 2023; revised manuscript received Jan. 4, 2024; accepted for publication Feb. 5, 2024; published online Mar. 8, 2024.

© The Authors. Published by SPIE and CLP under a Creative Commons Attribution 4.0 International License. Distribution or reproduction of this work in whole or in part requires full attribution of the original publication, including its DOI.

[DOI: [10.1117/1.APN.3.2.026005](https://doi.org/10.1117/1.APN.3.2.026005)]

1 Introduction

As one of the most important intrinsic properties of light, polarization builds the link between orthogonal electric vectors involving amplitude and phase. Polarized light has attracted tremendous attention in the optical community,¹ as evidenced by the rapid developments in advanced light source,^{2–4} display,^{5–7} and sensing.^{8–10} Traditional polarizers are usually bulky and have many limitations for optical integration. The emergence of metasurfaces, which consist of subwavelength scale meta-atoms, provides a new route to address this issue. In the past years, various metasurfaces have been widely explored to manipulate the phase^{11–16} and polarization of light.^{17–22} The metasurface optical element, which has the ability to manipulate the electric field in different directions, can be described mathematically using the Jones matrix.^{23,24} By engineering the materials

and geometrical parameters of a meta-atom or meta-molecule, it is possible to construct the corresponding Jones matrix.^{25,26} It has been demonstrated that by assembling appropriate meta-atoms into a unit, one can achieve an arbitrary polarization state (PS).^{27–31}

Despite the rapid development of nanofabrication technology, the imperfection of metasurface polarizers hinders their practical applications. To partially circumvent this constraint, we propose to experimentally retrieve the Jones matrix of an imperfect metasurface polarizer. This approach allows us to accurately determine each component of the metasurface polarizers' Jones matrix at specific wavelengths. As a proof of concept, we utilized the retrieved Jones matrix to experimentally verify the outgoing PS. Moreover, by arranging the dielectric meta-atoms in a judicious manner, we demonstrated the polarization image encryption and chiroptical holography using the metasurface polarizers. The proposed methodology in this work may greatly release the strict manufacturing requirements of the

*Address all correspondence to Guixin Li, ligx@sustech.edu.cn

metasurface optical elements and thus benefits a wide variety of applications of polarization optics.

2 Method and Results

2.1 Jones Matrix Decomposition

In conventional optics, in order to generate the arbitrary PS of light, some specific assembly of a linear polarizer and various wave plates are usually used in the light path. Recent studies show that a single metasurface which consists of subwavelength scale meta-atoms can be utilized to mimic the multiple optical elements in traditional optics.^{25,27} As shown in Fig. 1, the combination of two birefringent dielectric meta-atoms can be used to design the metasurface polarizers.²⁷ The Jones matrix J of the metasurface polarizer can be decomposed to the superposition of that of the two birefringent meta-atoms, which is shown as

$$J = \frac{1}{2}R(-\psi + 45 \text{ deg}) \begin{bmatrix} e^{-i2\chi} & 0 \\ 0 & e^{i2\chi} \end{bmatrix} R(\psi - 45 \text{ deg}) + \frac{1}{2}R(-\psi) \begin{bmatrix} 1 & 0 \\ 0 & -1 \end{bmatrix} R(\psi), \quad (1)$$

where χ and ψ are the ellipticity angle and the main axes angle of the PS of light, respectively. As shown in Figs. 1(a) and 1(b), the phase retardations of the fast and slow axes of the first meta-atom are -2χ and 2χ , respectively. The second meta-atom acts as a half-wave plate with phase retardations of 0 and π . The rotation angle of the first and second meta-atoms are $\psi - 45 \text{ deg}$ and ψ , respectively [Fig. 1(c)]. Therefore, by controlling the birefringence of the two meta-atoms, one can convert the incident light with arbitrary PS to any position (ψ, χ) on the Poincaré sphere [Fig. 1(d)]. However, once the phase retardations of a meta-atom deviate from the ideal values, the performance of the entire metasurface polarizer will deteriorate, as shown in Figs. 1(e) and 1(f). Among various factors, the imperfect etching depth and angle of the meta-atoms are the two common issues that will affect the performance of the metasurface polarizers. For the birefringent dielectric meta-atoms, which are designed to introduce proper phase retardation between two orthogonal electric field components, the planar geometrical parameters determine the introduced phase difference and the height affects the accumulated phase retardation. The etching angle and depth determine both the planar geometry and height of the meta-atoms, therefore, influence their optical functionalities and conversion efficiency. In this work, we assume that the etching process will not break the symmetry of the dielectric meta-atoms. These kinds of imperfections can

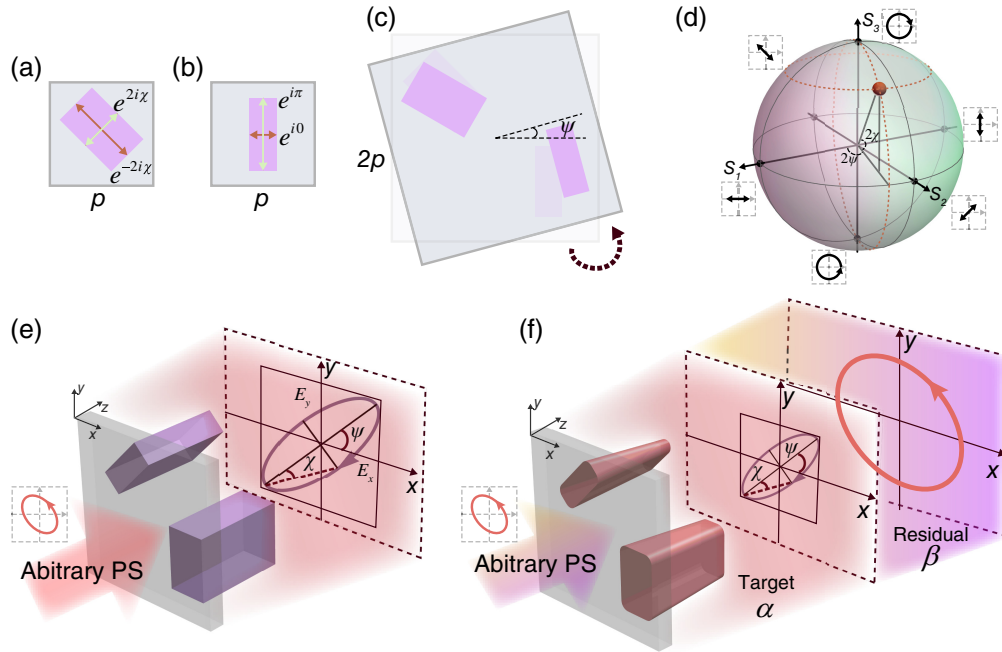


Fig. 1 Design concept of the metasurface polarizers. (a) A 45 deg counterclockwise rotated meta-atom with birefringence in a square lattice of period p . The phase retardation in different axes depends on the output PS's ellipticity angle χ . (b) A meta-atom, which is equivalent to a half-wave plate in a square lattice of period p . (c) The unit cell of a metasurface polarizer consists of two above-mentioned meta-atoms, which has a $2p$ period. The two meta-atoms fill the diagonal position and the rotation angle of these combinations depends on the output PS's main axes angle ψ . (d) Arbitrary PS on the Poincaré sphere can be described by the two parameters χ and ψ . (e) The schematic illustration of an ideal metasurface polarizer. Under the pumping of arbitrary PS, the metasurface polarizer can completely convert it into the target PS (ψ, χ) . (f) The schematic illustration of the imperfect metasurface polarizer. Only a certain percentage (α) of the transmitted light has the target PS (ψ, χ) , and the coefficient β corresponds to the residual due to the imperfections of the meta-atoms.

be regarded as planar plates and usually exert little effects on the polarization of the incident light. The corresponding Jones matrix can be rewritten as

$$J_{\text{real}} = \frac{\alpha}{2} R(-\psi + 45 \text{ deg}) \begin{bmatrix} e^{-i2\chi} & 1 \\ 1 & e^{i2\chi} \end{bmatrix} R(\psi - 45 \text{ deg}) + \beta \begin{bmatrix} 1 & 0 \\ 0 & 1 \end{bmatrix}, \quad (2)$$

where the α and β are the coefficients of the target Jones matrix and imperfection part, respectively. When β equals zero, the metasurface will become a perfect polarizer. Both the amplitude and phase of the two coefficients are associated with the wavelength of incident light and the imperfections of the meta-atoms.

First, we designed and fabricated the linear metasurface polarizer which consists of silicon nitride (SiN_x) meta-atoms sitting on a fused silica substrate. Through the Lumerical FDTD simulations at the wavelength of 660 nm, we built the phase retardation library of the birefringent meta-atoms with a height of 1400 nm [Fig. 2(a)]. The meta-atoms with length and width

varying from 100 to 380 nm are placed in the square lattices with periods of 400 and 450 nm in Figs. 2(b) and 2(c), respectively. According to the phase retardation library, we selected two types of meta-atoms to compose the meta-molecule. First, the first meta-atom as a half-wave plate was selected, corresponding to the latter part in Eq. (1), whose phase retardations of the fast and slow axes are ϕ_0 and $\phi_0 + \pi$, where ϕ_0 is an arbitrary real number. Then the second meta-atom corresponding to the former part in Eq. (1) was selected, in which phase retardations of the fast and slow axes are $\phi_0 - \phi$ and $\phi_0 + \phi$, where $\phi = 2\chi$ is determined by the target function of this polarizer. Based on the concept described in Fig. 1(c), different combinations of the meta-atoms were utilized to design three typical polarizers, including horizontal linear polarizer (LP-Pol-H, $l_1 = 210$ nm, $w_1 = 210$ nm, $l_2 = 160$ nm, $w_2 = 370$ nm, and $p = 400$ nm), left circular polarizer (LCP-Pol, $l_1 = 380$ nm, $w_1 = 110$ nm, $l_2 = 370$ nm, $w_2 = 150$ nm, and $p = 450$ nm), and right circular polarizer (RCP-Pol, $l_1 = 110$ nm, $w_1 = 380$ nm, $l_2 = 370$ nm, $w_2 = 150$ nm, and $p = 450$ nm). To verify the performance of the metasurface polarizers, the

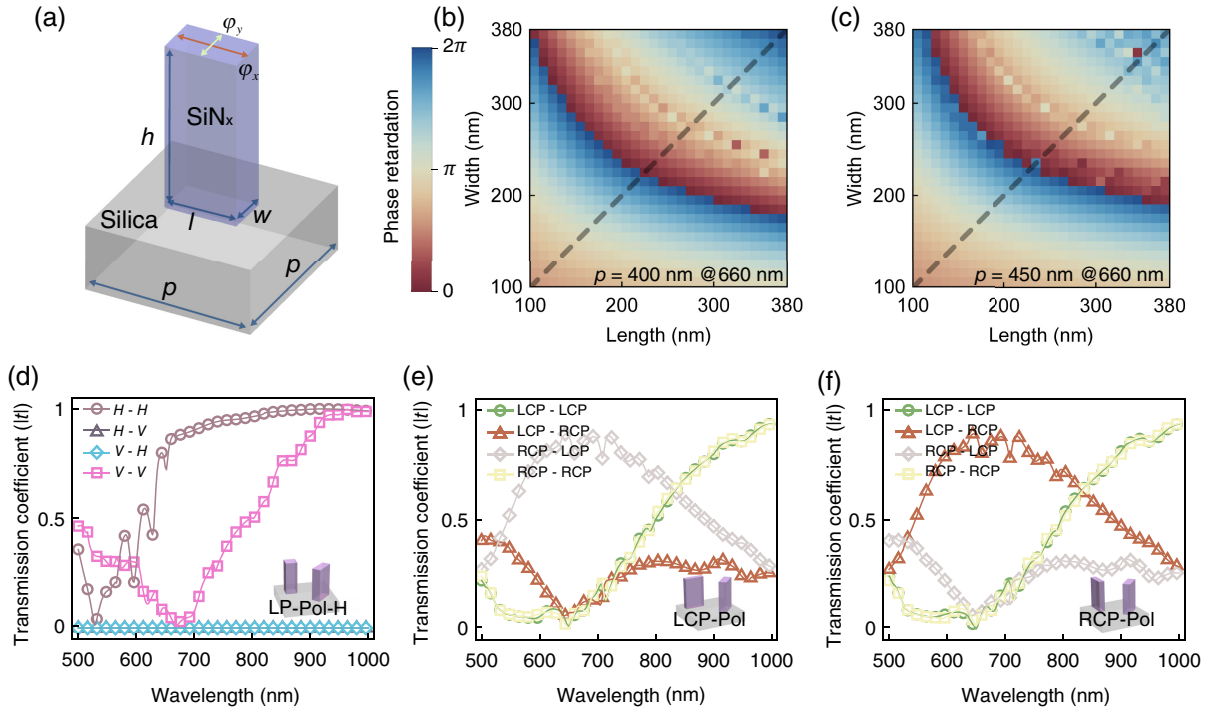


Fig. 2 Selection of the unit cell of metasurface polarizers. (a) Sketch of a SiN_x dielectric meta-atom, which is sitting on a fused silica substrate. ϕ_x and ϕ_y indicate the phase retardation that the transmitted light carries in the x and y axes, respectively. Structure parameters, h , l , and w , correspond to the height, length, and width of the meta-atom, respectively, and p is the period of the square lattice. (b), (c) Phase retardation library at the wavelength of 660 nm. The height h of the meta-atoms is kept at 1400 nm, and l and w are varied from 100 to 380 nm. The periods of the unit cell in panels (b) and (c) are 400 and 450 nm, respectively. (d)–(f) Simulation transmission coefficients of three kinds of metasurface polarizers, including horizontal linear polarizer (LP-Pol-H, $l_1 = 210$ nm, $w_1 = 210$ nm, $l_2 = 160$ nm, $w_2 = 370$ nm, and $p = 400$ nm), left circular polarizer (LCP-Pol, $l_1 = 380$ nm, $w_1 = 110$ nm, $l_2 = 370$ nm, $w_2 = 150$ nm, and $p = 450$ nm), and right circular polarizer (RCP-Pol, $l_1 = 110$ nm, $w_1 = 380$ nm, $l_2 = 370$ nm, $w_2 = 150$ nm, and $p = 450$ nm). For (d) LP-Pol-H, four combinations of polarization measurement schemes (horizontal polarization H and vertical polarization V) are calculated. H–H means that both the incident light and transmitted light are linearly polarized. Panels (e) and (f) show optical properties of the LCP-Pol and RCP-Pol. LCP and RCP: left- and right-circular polarizations.

polarization-dependent transmission spectra of the three metasurface polarizers were numerically calculated in the wavelength range from 500 to 1000 nm in Figs. 2(d)–2(f). For the linear metasurface polarizer with an optical axis along a horizontal (H) direction, it has a high polarization extinction ratio in the wavelength range between 650 and 700 nm.

From the calculated results, we can see that the bandwidths of these three kinds of polarizers are quite narrow, which will definitely limit the practical applications. To partially circumvent this issue, we experimentally retrieve the target Jones matrices from the imperfect metasurface polarizers. As shown in Fig. S1(a) (Sec. 1 in the [Supplementary Material](#)), we carried out the following optical measurements. The output from a supercontinuum laser is normally incident on the metasurface polarizers from the substrate side. The polarization ellipse of the transmitted light can be sketched by rotating the linearly polarized analyzer and recording the transmitted power (Fig. 3 and Sec. 1 in the [Supplementary Material](#)). To retrieve the four complex terms in the Jones matrix of a linear metasurface polarizer, six kinds of PSs of the incident light were used, including linear polarizations along H , V , 45 deg, 135 deg directions, left- and right-circular polarizations (LCP and RCP). By fitting the six measured ellipses (dot orange lines), the Jones matrix of an imperfect linear polarizer can be determined at each wavelength (Secs. 2 and 3 in the [Supplementary Material](#)). Using the measured Jones matrix of the metasurface polarizer (LP-Pol-H) and the six kinds of input PSs, we can calculate the corresponding polarization ellipses and their rotating directions (solid blue lines). In addition, it is shown that the above methodology can be applied to different wavelengths of the incident light. For example, at the wavelengths of 690 and 760 nm, where the Jones matrices are close to or deviate from the ideal ones, we find that the calculated polarization ellipses agree well with the experiment ones. By scanning the wavelengths of the incident light from 640 to 840 nm, we can experimentally extract the coefficients α and β of the target Jones matrix and imperfection part, respectively. The wavelength-dependent ratio of

$|\alpha/\beta|$ is shown in Sec. 4 in the [Supplementary Material](#), from which we can evaluate the level of imperfection of the metasurface polarizers. As shown in Sec. 5 in the [Supplementary Material](#), the optical properties of the circular metasurface polarizers (LCP-Pol and RCP-Pol) were characterized using the same methods as that in Fig. 3. Both the left- and right-circular metasurface polarizers exhibit good polarization effect between 600 and 700 nm. Notably, the circular metasurface polarizers act as both a half-wave plate and a polarization filter, which is distinguished from their conventional counterparts.

2.2 Polarization Image Encryption with Linear Metasurface Polarizers

We show that the linear metasurface polarizers can be used for polarization image encryption by delicately arranging the rotation angles of the meta-atoms in real space. The center of the rotation of each polarizer is the center of the unit cell with an area size of 800 nm \times 800 nm. Each unit contains two meta-atoms, this is to ensure that there are no additional coupling effects due to the rotations [Fig. 4(a)]. Next, we demonstrate the polarization information can be embedded into the “META” image capability by choosing the rotation angle $\varphi = 45$ deg, 135 deg, 0 deg, 90 deg [Fig. 4(b)]. The top-view and side-view scanning electron microscopy (SEM) images of the four characters are shown in Figs. 4(c) and 4(d). The geometrical parameters of the meta-atoms are the same as that in the LP-Pol-H metasurface polarizer. Then the polarization performance of the metasurfaces was characterized with the experimental setup depicted in Fig. 1(b) (see Sec. 4.1 and Fig. S1 in the [Supplementary Material](#) for more details). The combination of a linear polarizer LP1 and a quarter-wave plate was utilized to control the PS of the incident light, whereas the function of the second linear polarizer LP2 is to measure the polarization ellipse of the transmitted light.

Then we tested the polarization image encryption performance of the linear metasurface polarizers at working

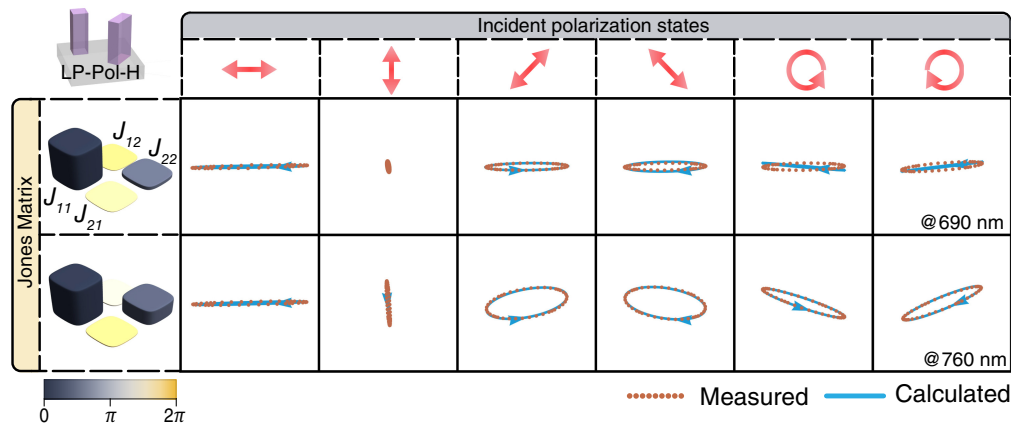


Fig. 3 Experimental retrieval of the Jones matrix of the linear metasurface polarizer. The PSs of the incident light include linear polarizations along H , V , 45 deg, 135 deg directions, and left- and right-circular polarizations (LCP and RCP). After passing through the LP-Pol-H metasurface, the polarization ellipses directions of the transmitted light at wavelengths of 690 and 760 nm were measured. The dot and solid lines correspond to the measured and calculated data, respectively. From the calculated results, we can obtain the spin directions of the electric fields, which are indicated by the arrows. Each element of the Jones matrix is shown by the bar charts, in which the height and color are associated with the amplitude and phase.

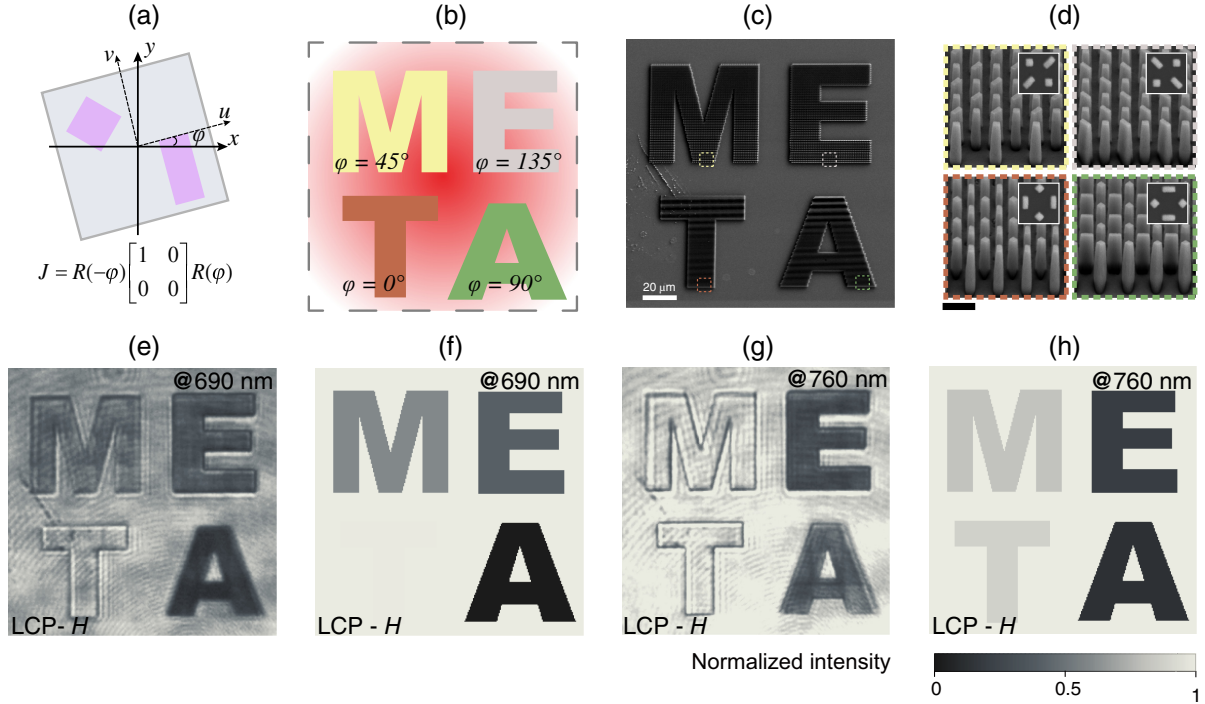


Fig. 4 Polarization image encryption with the linear metasurface polarizers. (a) A schematic drawing of a tilted linear metasurface polarizer, which is rotated by an angle φ . (b) The layout of the linear metasurface polarizers. For letters M, E, T, and A, the corresponding rotation angles are $\varphi = 45$ deg, 135 deg, 0 deg, and 90 deg, respectively. The red pattern represents the incident Gaussian beam. (c), (d) The scanning electron microscope (SEM) images of the metasurfaces. The scale bars of the SEM images are (c) 20 and (d) 1 μm , respectively. (e), (g) For incident light with LCP state, the intensity distribution of the four letters is measured at the wavelengths of 690 and 760 nm using a horizontal linear analyzer. (f), (h) The calculated intensity distribution of the four letters is based on the measured Jones matrix. The results in (e)–(h) are normalized to the maximum intensity values.

wavelengths of 690 and 760 nm, respectively. In the experiment, a circularly polarized Gaussian beam from the supercontinuum laser is normally incident onto the META image, and the normalized intensity of each letter was measured after passing through a linear analyzer with a fast axis along the horizontal direction. For the incident light at the wavelength of 690 nm [Fig. 4(e)], the contrast between the two perpendicular polarizer regions (letters: **T** and **A**) is distinct, indicating the high-polarization extinction ratio of the linear metasurface polarizers. As the fast axis of the designed linear metasurface polarizers in **M** and **E** has the projection angle of $\varphi = 45$ deg, 135 deg with respect to the horizontal axis, the intensity of these two letters is basically the same as each other according to the Malus's Law. When the wavelength of incident light is switched to 760 nm, the intensities of the four letters deviate from the theoretical values due to the existence of the residual light [Fig. 4(g)]. In Figs. 4(f) and 4(h), we show that the intensity distribution of the META image can be calculated through the measured Jones matrix of the linear metasurface polarizer (see Sec. 6 in the [Supplementary Material](#)). The calculated intensity distributions agree well with the ones captured by the CCD camera. Furthermore, by extracting the complex coefficients α and β from Eq. (2), the intensity ratio of the target polarization components and the residual one is obtained. The coefficients of the metasurface polarizer's Jones

matrices here act as the keys to revealing the useful information in the transmitted light.

2.3 Optical Holography with Circular Metasurface Polarizers

Based on the concept of geometric phase, we also demonstrated the spin-selective optical holography^{32–35} by engineering the meta-atoms' rotation angles, as shown in Figs. 5(a) and 5(b). For an ideal circular metasurface polarizer, when the meta-atom is rotated by an angle of φ , the transmitted light will carry a geometric phase of $2\sigma\varphi$, where $\sigma = \pm 1$ correspond to the left- and right-circular PSs of the incident light. The mechanisms can be explained by applying the Jones matrices of the left- and right-circular metasurface polarizers on the Jones vectors of the incident light with arbitrary PS, which are shown as

$$\frac{1}{2}R(-\varphi) \begin{bmatrix} -i & 1 \\ 1 & i \end{bmatrix} R(\varphi) \begin{bmatrix} E_x \\ E_y \end{bmatrix} = \frac{1}{2}e^{-2i\varphi}(-iE_x + E_y) \begin{bmatrix} 1 \\ i \end{bmatrix}, \quad (3)$$

$$\frac{1}{2}R(-\varphi) \begin{bmatrix} i & 1 \\ 1 & -i \end{bmatrix} R(\varphi) \begin{bmatrix} E_x \\ E_y \end{bmatrix} = \frac{1}{2}e^{2i\varphi}(iE_x + E_y) \begin{bmatrix} 1 \\ -i \end{bmatrix}, \quad (4)$$

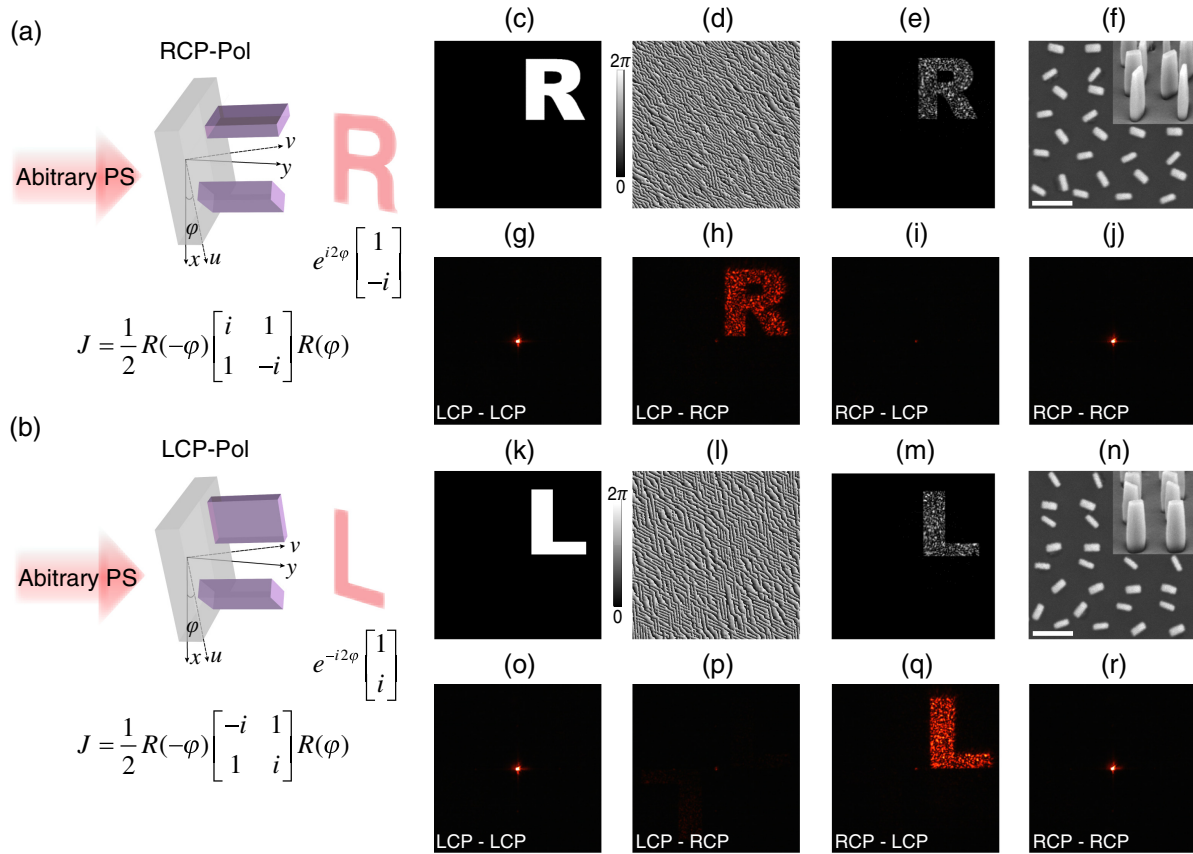


Fig. 5 Optical holography with circular metasurface polarizers. (a), (b) Schematics of the Fourier space holography based on RCP-Pol and LCP-Pol. The working wavelength is 700 nm. For the incident light with arbitrary PS, the circularly polarized output light carries a phase factor of 2φ , where φ is the rotation angle of the metasurface polarizer. (c), (k) The target intensity distribution of the holographic images. (d), (l) The calculated phase distributions of metasurface holograms. (e), (m) The reconstructed holographic images using the conditions in the experiment. (f), (n) The SEM images of RCP-Pol and LCP-Pol hologram devices (scale bar: 500 nm). The holographic images of (g)–(j) RCP-Pol and (o)–(r) LCP-Pol hologram devices were obtained under the measurements of four polarizer and analyzer (LCP and RCP) combinations.

where E_x and E_y are the electric fields of the incident light, and $[1, i]^T$ and $[1, -i]^T$ represent the left- and right-circular PSs of the transmitted light, respectively. It is worth noting that in order to reduce the coupling effects of the adjacent meta-atoms, the period of the unit cell is set to be $1.0 \mu\text{m}$ along both the x and y directions. Meanwhile, the geometrical parameters of the meta-atoms remain the same as those of the uniform metasurfaces in Fig. 2.

We designed and fabricated two kinds of phase-type metasurface holograms, based on the RCP-Pol [Figs. 5(c)–5(j)] and LCP-Pol [Figs. 5(k)–5(r)]. The phase maps [Figs. 5(d) and 5(l)] of the holographic images (“R” for the RCP-Pol, “L” for the LCP-Pol) were calculated using the commercial software VirtualLab Fusion. As shown in Figs. 5(e) and 5(m), the holographic images were reconstructed for a Gaussian beam (waist radius: $140 \mu\text{m}$ and $\lambda = 700 \text{ nm}$), which matches the experimental conditions. The SEM images of the circular metasurface polarizers are in Figs. 5(f) and 5(n). In the holography experiment [Fig. S2(c) in the [Supplementary Material](#)], the incident light from a supercontinuum laser is normally incident on the metasurfaces (see Sec. 4.1 for more details). By changing the

circular PSs of the incident light, the spin-selective holographic images of the RCP-Pol and LCP-Pol devices are shown in Figs. 5(g)–5(j) and Figs. 5(o)–5(r), respectively. As expected, the holographic images can only be observed in the LCP-RCP and RCP-LCP measurement schemes for the RCP-Pol and LCP-Pol devices, respectively. Benefitting from this spin selective transmission property, there is no twin image generation, which exists in the typical geometric phase-based metasurface holography. By introducing the phase gradient into the metasurface holograms, the converted polarized light is separated from the residual light. This also allows us to easily separate the holographic images and the residual light, which correspond to the target Jones matrix and residual part. The optical performance of the metasurface holograms was also carried out at 680 and 760 nm, and similar phenomena were observed (see Sec. 7 in the [Supplementary Material](#)).

3 Discussion and Conclusions

In summary, we have proposed a new strategy for retrieving the Jones matrix of an imperfect metasurface polarizer. Through

a series of polarization measurements, we can comprehensively characterize the optical properties of the metasurface polarizers. Moving from theory to practice, we fabricated and measured the real Jones matrices of three metasurface polarizers at different wavelengths. Utilizing the linear metasurface polarizers, we demonstrated the polarization image encryption in real space, where the real Jones matrix plays a critical role in separating the target polarization component and the residual. By introducing the concept of geometric phase into the design of circular metasurface polarizers, we also presented the spin selective optical holography phenomenon. In addition, there is a one-to-one correspondence between the incident PSs and the transmitted ones, which may enable us to achieve a full Stokes polarimetry by a single metasurface optical chip. The proposed Jones matrix retrieval approach opens a new route for extracting useful information from imperfect metasurface optical elements and may have important applications in polarization imaging,^{36,37} advanced light source,³⁸ information multiplexing,^{39,40} and so on. It should be noted that the traditional polarization optical elements are still playing important roles due to their high efficiency, extinction ratio, and wide bandwidth. Under specific application scenarios that requires small volume, light weight, and high integration level, the metasurface could be a promising platform. Thanks to the rapid development of nanofabrication, the large-scale fabrication of metasurfaces is compatible with the mature CMOS technology. By combining electron beam lithography, DUV projection lithography, and nanoimprinting technologies,^{41,42} the mass production costs can be greatly reduced in the future.

4 Appendix

4.1 Materials and Methods

4.1.1 Device fabrication

All the metasurface devices in this work were fabricated using the electron beam lithography and inductively coupled plasma etching processes. The procedures are as follows: a fused silica substrate with a 1400 nm thick silicon nitride layer, which was grown by plasma-enhanced chemical vapor deposition, was spin-coated with the positive tone electron beam resist and the charge dissipation solution, respectively. After baking the resist at a temperature of 180°C and the charge dissipation layer at a temperature of 90°C, the designed meta-atom patterns were written by exposing the resist with the electron beam lithography then developed in the MIBK/IPA 1:3 developer and washed in DI water. Afterward, a 20 nm thick chromium layer was deposited via the electron beam evaporation to fill the developed patterns, and the samples were immersed into the acetone for the lift-off process. The chromium patterns act as the hard mask in the inductively coupled plasma etching process (gas: CHF₃ and O₂), protecting the covered area from exposure to the plasma, and the silicon nitride meta-atoms were formed. Finally, the chromium residual was removed from the top of the meta-atoms using the chromium etchant.

4.1.2 Optical experiment

There are three optical setups for characterizing the metasurface polarizers' Jones matrix (Fig. S1 in the [Supplementary Material](#)). The incident light source is a supercontinuum laser (NKT), and the output wavelength ranging from 640 to 1100 nm is controlled by an acousto-optic modulator. All the

polarization states are defined when the incident light is viewed against the propagation direction of light. An assembly of a linear polarizer and a quarter-wave plate is used to obtain the LCP and RCP states of incident light. In the case of linear polarization measurement, one linear polarizer and one linear analyzer were used. The incident light is focused onto the metasurface polarizers from the substrate side by a lens with a focal length of $f = 100$ mm and the transmitted light is collected by a 10× objective lens. The power of the transmitted light was measured by a Thorlabs power meter. For the polarization image encryption measurement, the transmitted signals were captured by a CCD camera. For the optical holography experiment, the focal length of lens 1 is 250 nm which was used to generate a Gaussian beam with a waist radius of ~ 140 μm.

Disclosures

The authors declare no competing interest.

Code and Data Availability

The data of this study are available from the corresponding author upon reasonable request.

Acknowledgments

This work was supported by the National Key Technologies R&D Program of China (Grant No. 2022YFA1404301), the Zhangjiang Laboratory, the National Natural Science Foundation of China (Grant Nos. 91950114 and 12161141010), the Guangdong Provincial Innovation and Entrepreneurship Project (Grant No. 2017ZT07C071), the Guangdong Provincial Key Laboratory Program (Grant No. 2021B1212040001), and the Natural Science Foundation of Shenzhen Innovation Commission (Grant No. JCYJ20200109140808088).

References

1. D. H. Goldstein, *Polarized Light*, 3rd ed., CRC Press, Boca Raton (2017).
2. P. G. Kwiat et al., "New high-intensity source of polarization-entangled photon pairs," *Phys. Rev. Lett.* **75**(24), 4337–4341 (1995).
3. Y. Kozawa and S. Sato, "Generation of a radially polarized laser beam by use of a conical Brewster prism," *Opt. Lett.* **30**(22), 3063 (2005).
4. E. Matioli et al., "High-brightness polarized light-emitting diodes," *Light Sci. Appl.* **1**(8), e22 (2012).
5. M. De and L. Sévigny, "Polarization holography," *J. Opt. Soc. Am.* **57**(1), 110–110 (1967).
6. K. V. Chellappan, E. Erden, and H. Urey, "Laser-based displays: a review," *Appl. Opt.* **49**(25), F79–F98 (2010).
7. T. Badloe et al., "Liquid crystal-powered Mie resonators for electrically tunable photorealistic color gradients and dark blacks," *Light Sci. Appl.* **11**(1), 118 (2022).
8. K. Sassen, "The polarization lidar technique for cloud research: a review and current assessment," *Bull. Am. Meteorol. Soc.* **72**(12), 1848–1866 (1991).
9. A. C. S. Readhead et al., "Polarization observations with the cosmic background imager," *Science* **306**(5697), 836–844 (2004).
10. C. He et al., "Polarisation optics for biomedical and clinical applications: a review," *Light Sci. Appl.* **10**(1), 194 (2021).
11. N. Yu et al., "Light propagation with phase discontinuities: generalized laws of reflection and refraction," *Science* **334**(6054), 333–337 (2011).
12. L. Huang et al., "Dispersionless phase discontinuities for controlling light propagation," *Nano Lett.* **12**(11), 5750–5755 (2012).

13. D. Lin et al., “Dielectric gradient metasurface optical elements,” *Science* **345**(6194), 298–302 (2014).
14. A. Arbabi et al., “Dielectric metasurfaces for complete control of phase and polarization with subwavelength spatial resolution and high transmission,” *Nat. Nanotechnol.* **10**(11), 937–943 (2015).
15. G. Zheng et al., “Metasurface holograms reaching 80% efficiency,” *Nat. Nanotechnol.* **10**(4), 308–312 (2015).
16. H. Ren et al., “Complex-amplitude metasurface-based orbital angular momentum holography in momentum space,” *Nat. Nanotechnol.* **15**(11), 948–955 (2020).
17. N. Yu et al., “A broadband, background-free quarter-wave plate based on plasmonic metasurfaces,” *Nano Lett.* **12**(12), 6328–6333 (2012).
18. N. K. Grady et al., “Terahertz metamaterials for linear polarization conversion and anomalous refraction,” *Science* **340**(6138), 1304–1307 (2013).
19. C. Pfeiffer et al., “High performance bianisotropic metasurfaces: asymmetric transmission of light,” *Phys. Rev. Lett.* **113**(2), 023902 (2014).
20. Y. Yang et al., “Dielectric meta-reflectarray for broadband linear polarization conversion and optical vortex generation,” *Nano Lett.* **14**(3), 1394–1399 (2014).
21. S. Kruk et al., “Invited article: broadband highly efficient dielectric metadevices for polarization control,” *APL Photonics* **1**(3), 030801 (2016).
22. P. C. Wu et al., “Versatile polarization generation with an aluminum plasmonic metasurface,” *Nano Lett.* **17**(1), 445–452 (2017).
23. R. C. Jones, “A new calculus for the treatment of optical systems I. Description and discussion of the calculus,” *J. Opt. Soc. Am.* **31**(7), 488–493 (1941).
24. M. Born, E. Wolf, and A. B. Bhatia, *Principles of Optics*, 7th ed., Cambridge University Press, Cambridge (1999).
25. R. C. Devlin et al., “Arbitrary spin-to-orbital angular momentum conversion of light,” *Science* **358**(6365), 896–901 (2017).
26. J. P. Balthasar Mueller et al., “Metasurface polarization optics: independent phase control of arbitrary orthogonal states of polarization,” *Phys. Rev. Lett.* **118**(11), 113901 (2017).
27. S. Wang et al., “Arbitrary polarization conversion dichroism metasurfaces for all-in-one full Poincaré sphere polarizers,” *Light Sci. Appl.* **10**(1), 24 (2021).
28. Y. Bao et al., “Toward the capacity limit of 2D planar Jones matrix with a single-layer metasurface,” *Sci. Adv.* **7**(25), eabh0365 (2021).
29. Z. Shi et al., “Continuous angle-tunable birefringence with free-form metasurfaces for arbitrary polarization conversion,” *Sci. Adv.* **6**(23), eaba3367 (2020).
30. A. H. Dorrah et al., “Metasurface optics for on-demand polarization transformations along the optical path,” *Nat. Photonics* **15**(4), 287–296 (2021).
31. S. Lung, et al., “Complex-birefringent dielectric metasurfaces for arbitrary polarization-pair transformations,” *ACS Photonics* **7**(11), 3015–3022 (2020).
32. N. Mao et al., “Nonlinear vectorial holography with quad-atom metasurfaces,” *Proc. Natl. Acad. Sci. U. S. A.* **119**(22), e2204418119 (2022).
33. R. Zhao et al., “Multichannel vectorial holographic display and encryption,” *Light Sci. Appl.* **7**(1), 95 (2018).
34. Q. Song et al., “Broadband decoupling of intensity and polarization with vectorial Fourier metasurfaces,” *Nat. Commun.* **12**(1), 3631 (2021).
35. N. A. Rubin et al., “Jones matrix holography with metasurfaces,” *Sci. Adv.* **7**(33), eabg7488 (2021).
36. E. Arbabi et al., “Full-Stokes imaging polarimetry using dielectric metasurfaces,” *ACS Photonics* **5**(8), 3132–3140, (2018).
37. N. A. Rubin et al., “Matrix Fourier optics enables a compact full-Stokes polarization camera,” *Science* **365**(6448), eaax1839 (2019).
38. P.-N. Ni et al., “Spin-decoupling of vertical cavity surface-emitting lasers with complete phase modulation using on-chip integrated Jones matrix metasurfaces,” *Nat. Commun.* **13**(1), 7795, (2022).
39. B. Xiong et al., “Breaking the limitation of polarization multiplexing in optical metasurfaces with engineered noise,” *Science* **379**(6629), 294–299 (2023).
40. T. Chang et al., “Universal metasurfaces for complete linear control of coherent light transmission,” *Adv. Mater.* **34**, 2204085 (2022).
41. J. Kim et al., “Scalable manufacturing of high-index atomic layer–polymer hybrid metasurfaces for metaphotonics in the visible,” *Nat. Mater.* **22**, 474–481 (2023).
42. J. S. Park et al., “All-glass 100 mm diameter visible metalens for imaging the cosmos,” arXiv:2307.08186 (2023).

Guanqing Zhang received his Bachelor of Science degree from Sun Yat-sen University in 2018, his Master of Science degree from the Hong Kong University of Science and Technology in 2019, and his PhD in physics from the Hong Kong Baptist University in 2023. His main research direction is the design and fabrication of optical metasurfaces.

Zixian Hu received his Bachelor of Engineering degree from Fudan University, China, in 2020. He is currently a PhD student at the Southern University of Science and Technology, China. His research interests include linear and nonlinear optical metasurfaces, metasurface-based holography, and metasurface-based multifunctional terahertz radiation emitters.

Qichang Ma received his Bachelor of Science and Master of Engineering degrees from South China Normal University in 2019 and 2022, respectively. He is currently working toward his PhD at the Southern University of Science and Technology, China. His current research interests include optical metasurfaces devices and optical precise measurement.

Jiaming Huang is a postgraduate student at the Southern University of Science and Technology, China. He received his bachelor’s degree of engineering from the Southern University of Science and Technology, China, in 2022. His research interests include plasmonic metasurface and nanofabrication.

Junhong Deng received his bachelor’s degree of science from the Department of Applied Physics at the South China Agricultural University in 2012. He finished his PhD at the Hong Kong Baptist University in 2017. From 2017, he joined Photonic Materials and Metamaterials Laboratory at the Southern University of Science and Technology, China, as a research scholar and postdoctoral fellow. Now, he is a research assistant professor researching photonic metasurface, nonlinear optics, and nanofabrication.

Guixin Li is a professor in nanophotonics in the Department of Materials Science and Engineering, Institute for Applied Optics and Precision Engineering, Southern University of Science and Technology, China. He was awarded the 2019 Qiushi Outstanding Young Scholar of China. He has published 110 peer-reviewed papers in high-impact journals, such as *Nature Materials*, *Nature Nanotechnology*, *Nature Photonics*, *Nature Physics*, and *Nature Reviews Materials*.